Advanced Journal of Chemistry, Section A, 2025, 8(4), 809-824

Advanced Journal of Chemistry, Section A

journal homepage: www.ajchem-a.com

Original Research Article

Structural and Quantum Study of Newly Synthesized Methyl(Z)-3-((4-Fluorophenyl) Amino) But-2-Enoate

Salima Atlas [1], Koffi Senam Etsè [2], Zaragoza Verez Guillermo [3], Mohamed Maatallah [4], Abdessamad Tounsi [5], Mohamed Anouar Harrad [5,6]*

[1] *Chemical Science and Engineering Research Team (ERSIC), Sultan Moulay Slimane University, Beni-mellal 23000, Morocco*
[2] *Medicinal Chemistry Laboratory, Center for Interdisciplinary Research on Medicines (CIRM), University of Liège, B36 Av. Hippocrate 15 B-4000 Liege, Belgium*
[3] *Unidade de Difracción de Raios X, RIAIDT, Universidade de Santiago de Compostela, Campus VIDA, 15782 Santiago de Compostela, Spain*
[4] *Laboratory of Molecular Chemistry, Faculty of Sciences Semlalia, Cadi Ayyad University, Marrakech 40001, Morocco*
[5] *Environmental, Ecological, and Agro-Industrial Engineering Laboratory, Sultan Moulay Slimane University, Beni-mellal 23000, Morocco*
[6] *Regional center for Education Training and Formation, CRMEF 40000 Marrakech Safi, Morocco*

ARTICLEINFO

Article history

Submitted: 2024-08-02
Revised: 024-09-16
Accepted: 2024-10-10
ID: AJCA-2408-1623

DOI: **10.48309/AJCA.2025.471262.1623**

KEYWORDS

β-enaminoesters
X-ray diffraction
Hydrogen bonds analysis
DFT
Hirshfeld

ABSTRACT

Compound $C_{11}H_{12}NO_2F$ was obtained by reacting of 4-fluoroaniline with methyl acetoacetate, using $CoCl_2$ as a catalyst. X-ray structural analysis identified the structure of the synthetized enaminoester, and infrared spectroscopy and proton NMR complemented it. The *β*-enaminoester crystallized in the P21/c space group, which is symmetrical and monoclinic (Z=4) [a=6.5919(3)Å, b=15.9809(8)Å, c=10.1859(4)Å, β=105.3300(16) °; V = 1034.85 Å^3]. The crystal structure consists of alternating up and down $C_{11}H_{13}NO_2F$ molecules staked along with the b-axis. Van der Walls interactions keep the crystal structure together by looking at the weak hydrogen bonds of the N-H-O and C-H-O types inside the molecule. A high-level Density Functional Theory computation was performed on the investigated molecule, which was found to have a substantial correlation with the experimental data. Because of their high accuracy in determining the geometric structure of molecules, the B3LYP function and the 6-311+ G(2d,3p) basis set were chosen. The molecule chemical reactivity was evaluated by creating its Frontier Molecular Orbitals (FMOs) and the Molecular Electrostatic Potential surfaces (MEP). The global reactivity descriptors were computed using the FMOs energy levels, gaining further insight into the molecule's reactivity. The local reactivity was assessed by calculating the Fukui functions and dual descriptor indices. Analyses of Hirshfeld surface mapped over d_{norm} and shape-index were further used to identify the intermolecular interactions. The fingerprint histograms allow to show that H ···H (46.7%), O ···H (16.7%), and F ···H (14.2%) contacts are the dominant interactions in the crystal packing of the investigated molecule.

* Corresponding author: Harrad, Mohamed Anouar
✉ E-mail: ma.harrad@yahoo.fr

GRAPHICAL ABSTRACT

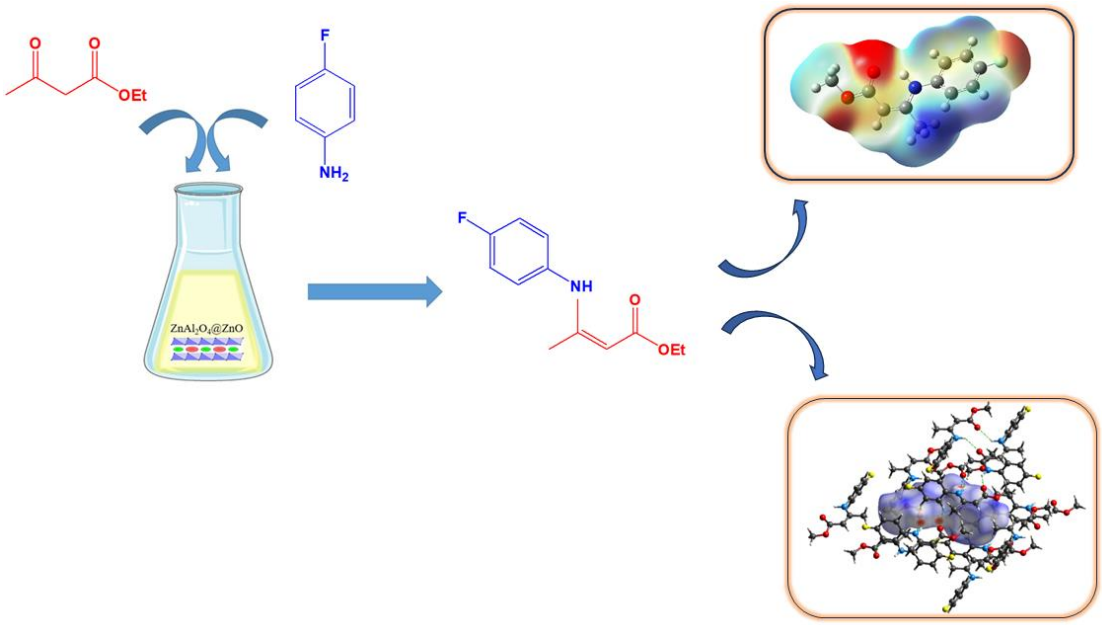

Introduction

β-enaminoesters are a significant class of organic compounds, widely used in synthetic and medicinal chemistry. They are characterized by an enamine group adjacent to an ester group, which gives them unique electronic properties that facilitate various chemical transformations [1,2]. Biologically, *β*-enaminoesters are highly important due to their substantial bioactivity across a range of pharmacological properties. For example, some *β*-enaminoesters have shown potential as acetylcholinesterase inhibitors, making them candidates for treating neurodegenerative diseases like Alzheimer's [3-6]. They also have antimicrobial properties useful for developing new antibiotics, antiviral properties effective against viruses like influenza and HIV, and anticancer potential by inducing apoptosis and inhibiting cell proliferation in various cancer cell lines. These activities underscore the importance of *β*-enaminoesters in drug discovery and development. Traditionally, *β*-enaminoesters are synthesized through the condensation of esters with amines under acidic or basic conditions. Recently, catalytic methods have become prominent, offering efficient, sustainable, and selective synthesis routes [7-11]. In addition, the compound 3-chloro-4-((4-bromophenyl) amino) pent-3-en-2-one was prepared and identified using spectroscopic techniques. Its structure was confirmed through X-ray diffraction analysis, showing a strong hydrogen bond and 38.7% of the total Hirshfeld surface. Quantum chemical calculations using density functional theory (DFT) confirmed the optimized molecular structure and high kinetic and thermodynamic stability of the studied *β*-enaminone [12]. This study focuses on the theoretical analysis of the structure of methyl-(Z)-3-((4-fluorophenyl)-amino)-but-2-enoate.

The synthesis involves the condensation reaction of 4-fluoroaniline and ethyl acetoacetate, catalyzed by cobalt (II) chloride ($CoCl_2$) at room temperature under solvent-free conditions [12], and the structural properties of the synthesized compound are examined through theoretical calculations using Density Functional

Theory (DFT) at the B3LYP/6–311+G(2d,3p) level. These calculations provide detailed insights into the electronic structure, stability, and reactivity of the molecule. By comparing the theoretical results with experimental data, we aim at validating the computational models and gain a deeper understanding of the molecular characteristics. Further analysis includes the calculation of Frontier Molecular Orbitals (FMOs) and Molecular Electrostatic Potential (MEP) surfaces. FMOs are crucial for predicting the molecule's reactivity and interaction with other chemical species, while MEP surfaces offer a visual representation of charge distribution, identifying potential sites for electrophilic and nucleophilic attacks. These analyses are complemented by the calculation of global reactivity descriptors, such as chemical potential, chemical hardness, softness, electrophilicity, and nucleophilicity indices, using FMO energies. These descriptors provide comprehensive information about the molecule's chemical reactivity and stability. In addition, the intermolecular interactions within the synthesized compound are investigated through Hirshfeld Surface Analysis (HSA). This technique offers a detailed view of the molecular interactions within the crystal structure, highlighting the contributions of various interactions to the compound's stability. By integrating experimental synthesis with advanced theoretical analysis, this study aims at providing a thorough understanding of the structural and electronic properties of methyl-(Z)-3-((4-fluorophenyl)-amino)-but-2-enoate.

The findings, not only enhance our knowledge of *β*-enaminoesters, but also pave the way for future research into their potential applications in medicinal chemistry and other fields.

Materials and Instruments

The solvents and other metals' chloride used were of high purity, purchased from Janssen Chemica, and Sigma-Aldrich, and utilized just as it arrived, such as $CoCl_2 \cdot 9H_2O$, ethyl acetoacetate, and 2,4,6-Trimethylaniline. The ^{1}H- and ^{13}C-NMR spectra were recorded on a Bruker Avance 300 spectrometer at 300 MHz and 75 MHz, respectively, in $CdCl_3$ solvent. Fourier-transform infrared (FTIR) spectra were obtained utilizing a Nicolet is 5 Thermo scientific spectrometer. Pellets were composed of 100 mg of finely powdered KBr and 2 mg of the sample. Melting points were determined on Banc Kofler apparatus.

Synthesis and crystallization

To a magnetically stirred mixture of the ethyl acetoacetate (5 mmol) and *p*-fluoro-aniline (5 mmol), $CoCl_2 \cdot 6H_2O$ (0.25 mmol) was added and the reaction mixture was stirred at room temperature for the appropriate time (15 min). At the end of the reaction, 10 mL of distilled water was added to the residue and extracted with diethyl ether (3 × 25 ml). The organic layer was dried over Na_2SO_4. The solvent was removed under reduced pressure, the pure *β*-enaminoester was obtained by column chromatography over silica gel using hexane/ethyl acetate as eluent. The pure product obtained as shiny crystals with a yield of 80% (Scheme 1). m.p.: 88-90 °C. FT-IR (KBr) ῡ (cm^{-1}): 3276, 3110, 1605, 1500, 1435, 967, and 689, 614. ^{1}H-NMR shifts ($CdCl_3$) d, ppm: 1.77 (s, 3H), 3.52 (s, 3H), 4.55 (s, 1H), 6.83-6.93 (m, 4H), and 10.12 (br s, 1H, NH). ^{13}C-NMR shifts ($CdCl_3$) δ, ppm: 19.94, 50.14, 85.46, 115.66, 115.96, 120.25, 125.7, 135.2, 158.76, 162.01, and 170.70. Methyl (Z)-3-((4-fluorophenyl) amino) but-2-enoate has been prepared in accordance with the reported method [11]. The condensation reaction of ethyl acetoacetate, and fluorophenyl leads to the formation of the corresponding ⍰-enaminoester with a very good yield 80%, in the presence of $CoCl_2$ as a catalyst, at room temperature under free-solvent conditions [11].

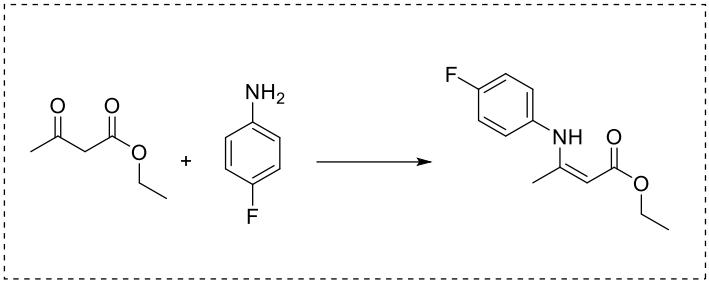

Scheme 1. Synthesis of methyl (Z)-3-((4-fluorophenyl) amino) but-2-enoate.

X-ray structure analysis and refinement

For the crystal structure determination, the previously reported procedure was used [13]. Briefly, the data were collected by applying the omega and phi scans method on a Bruker D8 Venture PHOTON III-14 diffractometer using INCOATEC multilayer mirror monochromated with MoKα radiation (λ=0.71073 ˚A). Computing data and reduction were made with the APEX3 [14]. The structure was solved using SHELXT [15], and finally refined by full-matrix least-squares basedon F2 by SHELXL [16]. An empirical absorption correction was applied using the SADABS program. Software used to molecular graphics: ORTEP for Windows [17]. WinGX Software was used for publication routines [18] and mercury [19] as well as to prepare material for publication.

Crystal and experimental data for methyl (Z)-3-((4-fluorophenyl) amino) but-2-enoate were listed in Table 1. Selected geometric parameters for (Z)-3-((4-fluorophenyl)-amino)-but-2-enoate were listed in Table 1,2. Crystallographic data for the structural analysis of methyl-(Z)-3-((4-fluorophenyl)-amino)-but-2-enoate have been deposited at the Cambridge Crystallographic Data Center, CCDC No 2323343 (https://www.ccdc.cam.ac.uk, email: deposit@ccdc.cam.ac.uk).

Computational methods

In this study, DFT method was used with the Lee-Yang-Parr exchange correlation functional (B3LYP) with three Becke parameters and the base set 6-311+G(2d,3p) [20]. The quantum calculation was performed with the Gussian 09 program [21]. The frontiers molecular orbitals (FMOs), the highest occupied molecular orbital (HOMO) and the lowest unoccupied molecular orbital (LUMO) have been identified, as well as their corresponding energies. The main global indices of chemical reactivity namely are the chemical electronegativity (χ), chemical potential (μ), global hardness (η), global softness (σ) electrophilicity index (ω), nucleophilicity (ε), and additional electronic charge (ΔN). These global indices were calculated on the basis of the energies of the orbitals of the shapes and using the equation cited in the literature [22-24]. The molecular electrostatic potential (MEP) was also examined to study the active sites of the compound in question and the possible interactions through the nucleophilic and electrophilic centers. At the same level of calculation, the NMR of the proton ^{1}H was determined as the structural optimization exploring the gauge independent atomic orbital (GIAO) method [25].

To better understand and visualize the intermolecular interactions in our compound, a Hirshfeld Surface Analysis (HSA) was calculated with the related 2D finger point plots using Crystal Explorer [26].

Results and Discussion

Molecular structure description

X-ray crystallography

The single crystal methyl-(Z)-3-((4-fluorophenyl)-amino)-but-2-enoate, picked for X-ray diffraction analysis has the crystal dimensions 0.14×0.11×0.08 mm at 100 K. This compound crystallizes in the monoclinic space group P21/c with Z = 4, a=6.5919(3) Å, b=15.9809(8) Å, c=10.1859(4) Å, α=90°, β=105.3300(16) °, γ=90°, and V=1034.85 Å^3. The crystal structure was determined using 2028 reflections, adhering to the [Fo>4σ(Fo)] criterion. This resulted in a reliability factor of R = 0.0392. Table 1 presents all the crystal, collection, and refinement data obtained for this sample at 100(2) K. The ORTEP representation crystal data, conditions of data collection, and the diffraction parameters are illustrated in Figure 1 (a) and Tables 1 and 2, respectively. Crystallographic analysis revealed that the nitrogen and fluorine atoms are planar with the aromatic carbons (C6, C_7, C_8, C_9, C_{10}, and C_{11}). The aminopent-3-en-2-one chain forms a second plan (C_1, C_2, C_3, C_4, C_5, and N_1) and the angle between the two plans is 45.97°. All hydrogen bonds (Å) reported in table 3 (N1—H1N—O2: 2.132(15); N1—H1N—O2^{i}: 2.390(16); and C11—H11—O2^{ii}: 2.4500) are responsible for the stabilization of the compound. A strong intramolecular O---H-N hydrogen bond is observed with a bond distance of 2.038 Å (acceptor - donor). The crystal appears to be stabilized by non-classical C-H---O bonds (Figure 1(b), (c), (d), and (e)). The ability of the molecule to form certain types of intermolecular interactions is the key factor for the construction of the crystal packing. Indeed, the biological activity depends on the formation of intermolecular interactions between the target molecule and the corresponding receptor, hence the importance of the study of these intermolecular interactions.

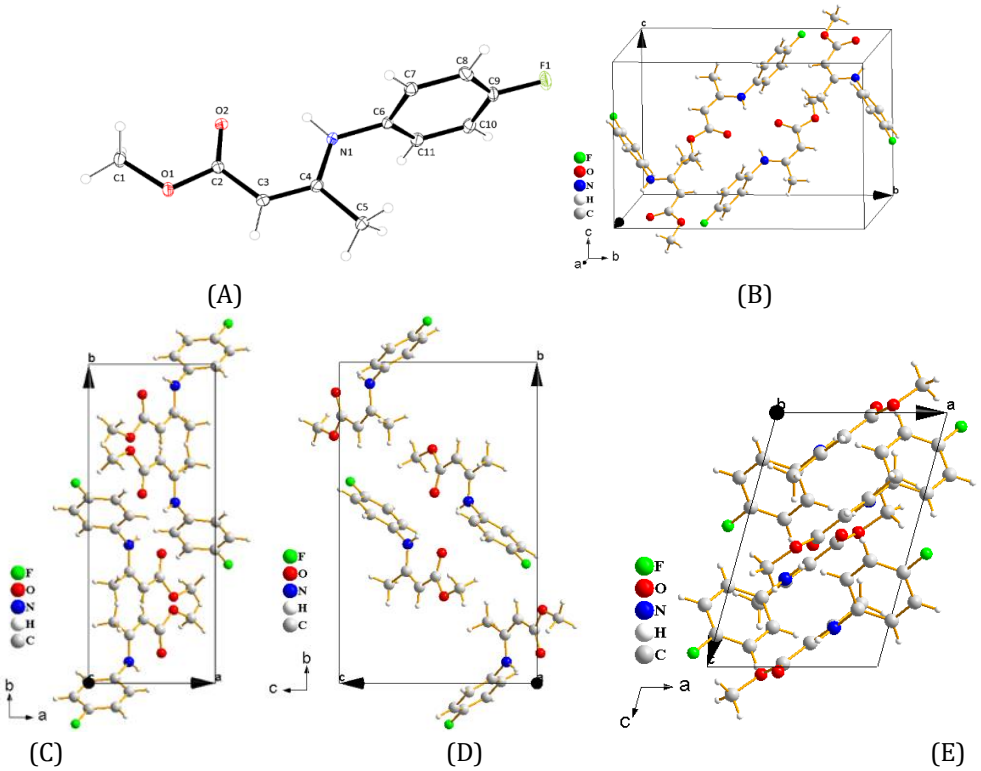

Figure 1. (a) ORTEP of methyl (Z)-3-((4-fluorophenyl) amino) but-2-enoate, (b) (the thermal ellipsoids are set at a 50% probability level), (c) projection along a crystallographic axis, (c) projection along c crystallographic axis, and (e) projection along crystallographic axis,

Table 1. Crystal data and summary of measurement parameters for $C_{11}H_{12}FNO_2$

Chemical formula	**$C_{11}H_{12}FNO_2$**
Formula weight	209.22 g/mol
Crystal system	Monoclinic
Space group	$P2_1/c$
Unit cell dimensions	a =6.5919(3) Å α= 90°
	b =15.9809(8) Å β=105.3300(16)
	c =10.1859(4) Å γ=90°
Volume	1034.85 Å^3
Z	4
μ mm^{-1}	0.104
Cryt. Density (g/cm^3)	1.343
F000	440
Radiation type	Mo *K*α
λ (Å)	0.71073
Crystal sizes (mm)	0.14 × 0.11 × 0.08
$\theta_{min} - \theta_{max}$ (°)	2.43 - 28.28
Data collection	
Diffractometer	Bruker D8 VENTUREPHOTON III- 14
Absorption correction	Muti-scan SADABS2016/2–Bruker AXS area detector scaling and absorption correction
T (K)	100(2)
Tmin, Tmax	0.986, 0.992
R	0.0392 for 2028 for Fo > 4sig (Fo)
Rall	0.0541 for all 2566 data
wR2/wR2_all	0.0921/0991
Index ranges	-8 ≤ h ≤8; -21≤k ≤21; 13 ≤l ≤13
GooF = S	1.053
Restrained GooF	1.053 for all data
Refined parametres	141 using 0 restraints
$\Delta\rho_{min}$ (eÅ^3), $\Delta\rho_{max}$ (eÅ^3)	0.259, -0.223

Hirshfeld surfaces analysis (HAS)

For better understating of packing forces Hirshfeld surfaces and fingerprint plots analysis using Crystal Explorer is performed [27]. The Hirshfeld molecular surfaces in the crystal structure are constructed on the basis of the electron distribution calculated as the sum of the electron densities of the spherical atoms [28]. The 2D fingerprint plots are displayed by using the translated 1.0 –3.0 Å view with the de and di distance scales displayed on the graph axes. To gain comprehensive insights into the underlying packing forces, a Hirshfeld surface analysis was conducted. This analytical technique enables the identification of significant contributions from non-polar particles or weak polar interactions within crystalline structures. It delineates regions or atoms on one molecular surface that engage in noteworthy interactions with neighboring molecules. The Hirshfeld surface encasing a molecule comprises points where the electron density of the molecule being examined equals the cumulative contribution from

surrounding molecules. Each point on the Hirshfeld iso-surface is associated with two distances: (di) denotes the distance between the point on the surface and the inner nuclei, while (de) represents the distance from the surface towards the outer nuclei. Furthermore, the 3D surface norm, which is adjusted for atom size, is depicted using a standardized color scale ranging from -0.24 Å (red) to 1.33 Å (blue). In addition, the aspect ratio is characterized within the interval of -0.99 to 2.70, and the curvature is delineated within the range of -4.00 to 0.4. Figures 2a-c display the Hirshfeld molecular surfaces, featuring attributes such as d_{norm}, aspect ratio, and curvature, specifically pertaining to the enaminoester molecule. The color encodes the normalized distance between nuclei, facilitating the easy identification of the strength of close interactions present in the crystalline packing. The color scale is designed in a way that the negative value of d_{norm} is visualized in red, indicating contacts shorter than the sum of Van der Waals radii.

Table 21 . X-ray diffraction and optimized geometrical parameters of methyl (Z)-3-((4-fluorophenyl) amino) but-2-enoate crystal structure obtained at B3LYP/6-311+ G(2d,3p) levels of theory

Bond length	**Exp. value**	**Calc. value** B3LYP/6-311+ G(2d,3p)	**Angles (°)**	**Exp.value**	**Calc. value** B3LYP/6-311+ G(2d,3p)
F1—C9	1.3626(14)	1,356	C2—O1—C1	116.71(10)	116,1025
O1—C2	1.3538(15)	1,357	C4—N1—C6	123.6(1)	129,673
O1—C1	1.4389(15)	1,435	O2—C2—O1	121.91(11)	121,4568
O2—C2	1.2265(15)	1,231	O2—C2—C3	126.62(11)	126,153
N1—C4	1.3533(16)	1,364	O1—C2—C3	111.47(11)	112,3889
N1—C6	1.4312(15)	1,4122	C4—C3—C2	124.00(12)	123,198
C2—C3	1.4332(17)	1,442	N1—C4—C3	123.22(11)	120,988
C3—C4	1.3657(17)	1,373	N1—C4—C5	117.09(11)	119,478
C3—H3	0.9500	1,09	C3—C4—C5	119.68(11)	119,5166
C4—C5	1.5014(17)	1,5057	C4—C5—H5	109.500	109,5489
C6—C11	1.3879(18)	1,400	C11—C6—C7	119.84(11)	118,818
C6—C7	1.3892(18)	1,402	C11—C6—N1	120.33(11)	122,902
C7—C8	1.3926(18)	1,3908	C7—C6—N1	119.83(11)	118,1806
C8—C9	1.375(2)	1,3859	C6—C7—C8	120.40(12)	120,93
C9—C10	1.374(2)	1,3849	C9—C8—C7	117.97(12)	118,7016
C10—C11	1.3887(18)	1,3927	F1—C9—C10	118.33(12)	119,030
			F1—C9—C8	118.53(12)	119,055
			C10—C9—C8	123.14(12)	121,9123
			C9—C10—C11	118.28(12)	118,965
			C6—C11—C10	120.33(12)	120,639

Table 3. Hydrogen bonding geometry (Å and °) for methyl (Z)-3-((4-fluorophenyl) amino) but-2-enoate compound

D*—H···*A	***D*—H (Å)**	**H···*A* (Å)**	***D*···*A* (Å)**	***D*—H···*A* (º)**
N1—H1N—O2	0.866(16)	2.132(15)	2.7837(13)	131.6(13)
N1—H1N—O2^{i}	0.866(16)	2.390(16)	3.0778(14)	136.7(13)
C11—H11—O2^{ii}	0.9500	2.4500	3.2746(16)	144.900

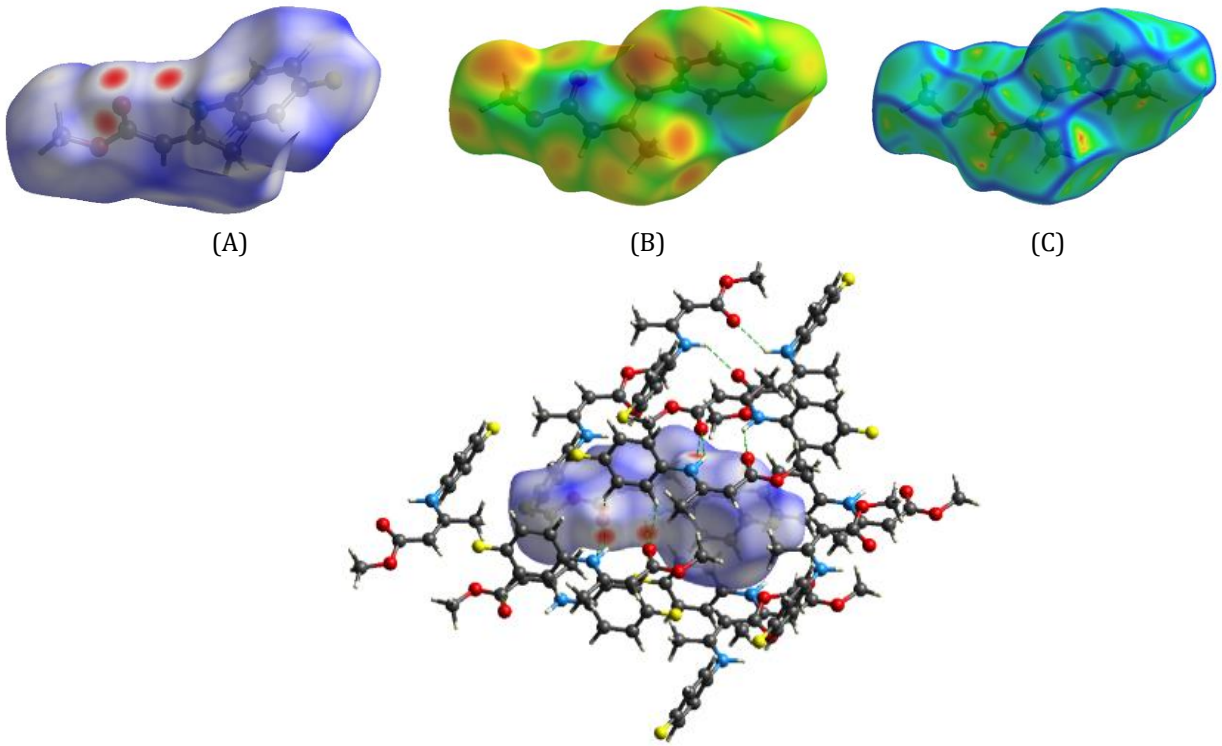

Figure 2. Hirshfeld surface mapped for methyl (Z)-3-((4-fluorophenyl) amino) but-2-enoate with (a) view of the d_{norm} (b) shape index, (c) curvedness, and (d) Hirshfeld surface mapped with d_{norm} (disposition of three approximate molecules).

White color visualizes intermolecular distances close to Van der Waals contacts with d_{norm} equal to zero. Contacts longer than Van der Waals radii are visualized in blue. As anticipated, the larger red patches correspond to the presence of hydrogen bonding contacts (O···H), which bring participating atoms closer than the sum of Van der Waals radii (Figure 3a). The shape index (3b) and curvature (3c) provide information on shape and extent. Larger areas reflect low curvature values, while areas of pronounced curvature indicate interactions between neighboring molecules. Fingerprint plots are useful for identifying the specific atom associated with close contacts [29]. 2D fingerprint plots revealed that the main intermolecular interactions in the enaminoester molecule were C–H, C–H–H, F–H, and C=O–H interactions (Figure S4a). The ability of the nitrogen atom to participate in hydrogen bonding depends largely on the availability of lone pairs. In the methyl (Z)-3-((4-fluorophenyl) amino) but-2-enoate structure, nitrogen has a substituent on the aromatic ring (fluorine), capable of resonating with the nitrogen's lone pair electrons, thereby reducing the availability of the lone pair. Non-classical C–H–H interactions contribute the most significantly to the total Hirshfeld surface (46.7%). The shortest contact is approximately 0.98 Å, corresponding to O-H/H-O interactions representing 16.7% of the total. Hirshfeld surface of the molecule, Figures 3a-e show the contribution of various contacts in the crystal structure of the enaminoester.

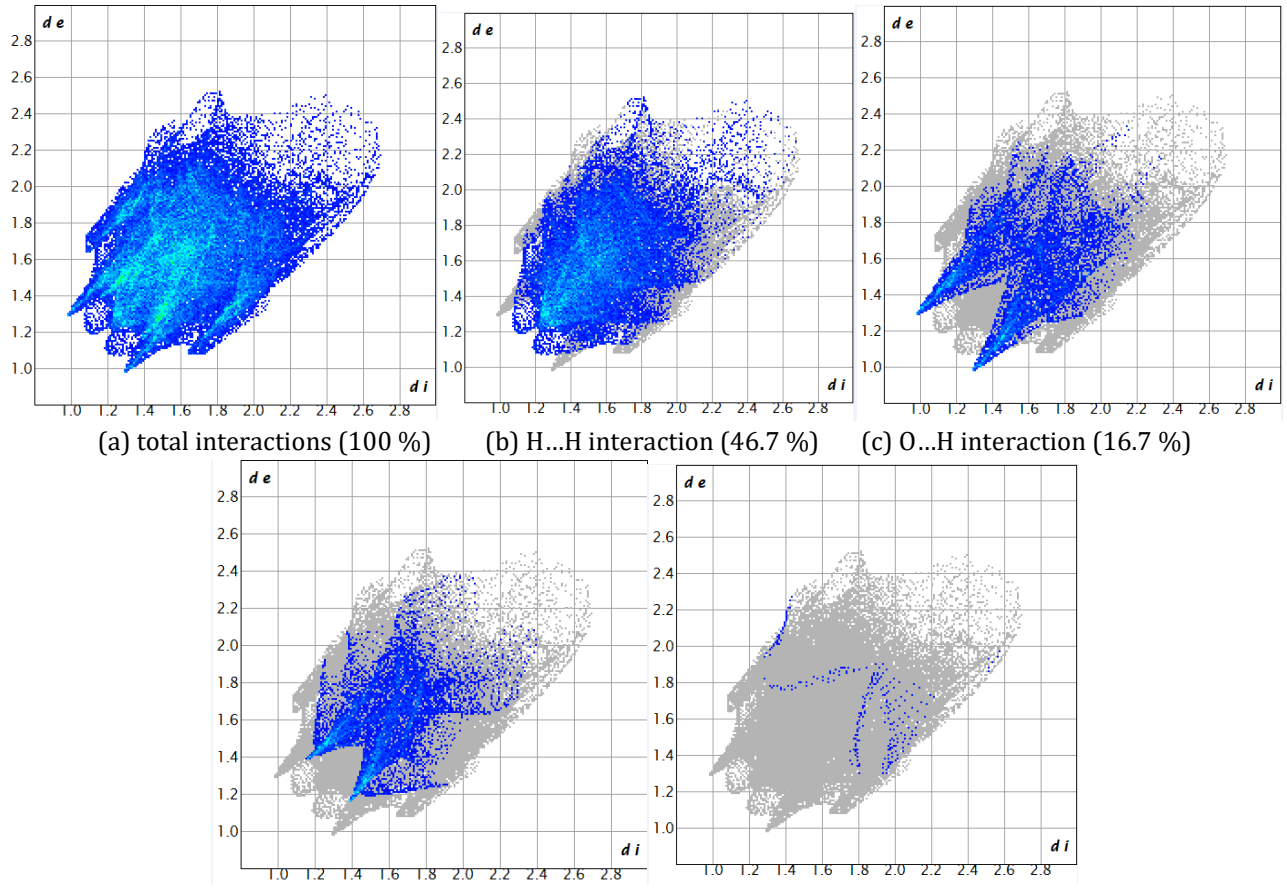

(a) total interactions (100 %) (b) H…H interaction (46.7 %) (c) O…H interaction (16.7 %)

(d) F…H interaction (14.2 %) (e) N-H interaction (0.4 %)

Figure 3. 2D Fingerprint plots of methyl (Z)-3-((4-fluorophenyl) amino) but-2-enoate showing interactions.

Table 4. Experimental and calculated IR (cm^{-1}) of methyl (Z)-3-((4-fluorophenyl) amino) but-2-enoate

	Experimental	Calculated (B3LYP/6-311+ G(2d,3p))
νN-H	3276	3388,77
νC=O	1605	1665,90
νC=C	1500, 1435	1524,93

Table 5. Experimental and computed ^{1}H-NMR of methyl (Z)-3-((4-fluorophenyl) amino) but-2-enoate

^{1}H-NMR	Exp. value δ(ppm)	Calc. value (B3LYP/6-311G+(2d, p)) δ(ppm)
(br s, 1H, NH)	10.12	10,24
(m, 4H-Ar)	6.83-6.93	6,65-6,75
(s, 1H, -C=C-H)	4.55	4,5
(s, 3H, O-CH_3)	3.52	3,5
(s, 3H)	1.77	1,68

Spectroscopic studies

The enaminoester's IR frequencies were computed at the computational levels of (B3LYP/6-311+ G(2d,3p)). Table 4 indicates both simulated and experimental frequencies. Since only these stretching IR vibrations have higher strengths in the IR region than other vibrations, the vibrational modes corresponding to N–H, C=C, and C=O stretching have been shown. To address systematic computational oversights (caused by the overestimation of electron correlation owing to neglect), it is extremely common practice to apply a scaling factor to calculated frequencies. It is noted that all frequencies in the computational findings of this enaminoester are overstated, and any potential N–H···O interactions are disregarded. The reason for the discrepancy between theoretical and experimental frequencies is that no interaction with the surrounding space was considered during computations yet.

The comparison of ^{1}H-NMR spectrum of the product with that of the methyl (Z)-3-((4-fluorophenyl) amino) but-2-enoate is shown in Figure S4. One essential method for characterizing synthesized compounds is ^{1}H-NMR. Table 5 displays computed and experimental ^{1}H-NMR data (in ppm reference to trimethylsilane). While theoretical computations were also conducted in a $CdCl_3$ environment, experimental chemical shifts were documented in a $CdCl_3$ solvent. For DFT calculations at B3LYP/6-311G + (2d, p), computed NMR agrees well with experimental findings. An average of the calculated chemical shifts is used for addressing variance in computed proton NMR since this computational approach has limitations in interpreting methyl protons in the isoelectronic environment.

Molecule structure optimization

The optimized geometric structure of methyl (Z)-3-((4-fluorophenyl) amino) but-2-enoate, obtained with the B3LYP functional and the 6-311+G(2d,3p) basis set, is demonstrated in Figure 4. This structure in terms of quantum calculations is quite similar to the one derived from the crystallographic investigations. Table 2 lists the chosen geometric parameters, which included bond lengths and angles, that were ascertained using X-ray diffraction (XRD) and DFT calculations. The geometric parameters are determined to be almost the same upon comparison. Minor disparities are noted, though, mostly because of the variations in the molecular environment. Indeed, X-ray crystallography was used to study the structure of the title molecule in the crystalline phase, whereas DFT calculations were conducted on an isolated molecule in the gas phase. The calculated bond lengths for F1-C9, O1-C2, O1-C1, O2-C2, N1-C4, and C3-C4 in the optimized geometry are 1.356Å, 1.357Å, 1.435Å, 1,231Å, 1,364Å, and 1,373Å, respectively, while the XRD structure values are 1.363(14)Å, 1.354(15)Å, 1.439(15)Å, 1.227(15) Å, 1.353(16) Å, and 1.366(17)Å. Regarding the bond angles, the DFT calculations have given values of 116.103°, 121.457°, 126.153°, 119.517°, 118.181°, and 119,055° for the angles C2—O1—C1, O2—C2—O1, O2—C2—C3, C3—C4—C5, C7—C6—N1, and F1—C9—C8, which is very close to the values obtained by XRD (116.71(10)°, 121.91(11)°, 126.62(11)°, 119.68(11)°, 119.83(11)°, and 118.53(12)° degrees, respectively). Thus, despite the disparities in the molecular medium, a satisfactory correlation was observed between the values obtained by DFT calculations and those by XRD. The agreement between the experimental and calculated data is evident in these results.

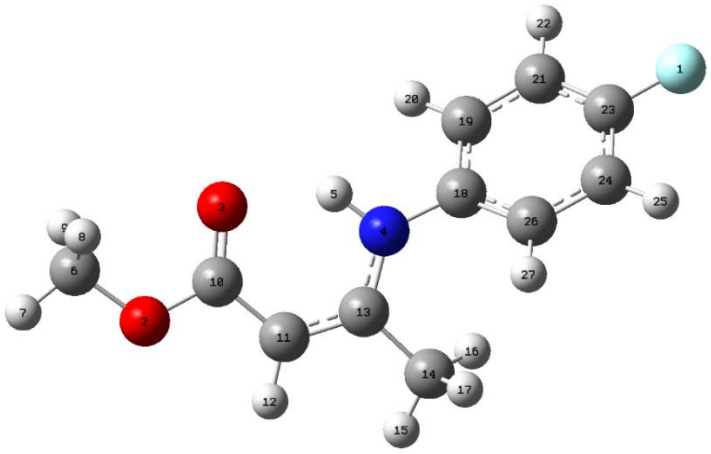

Figure 4. Optimized geometry of methyl (Z)-3-((4-fluorophenyl) amino) but-2-enoate at B3LYP/ 6-311+G(2d,3p) level of theory.

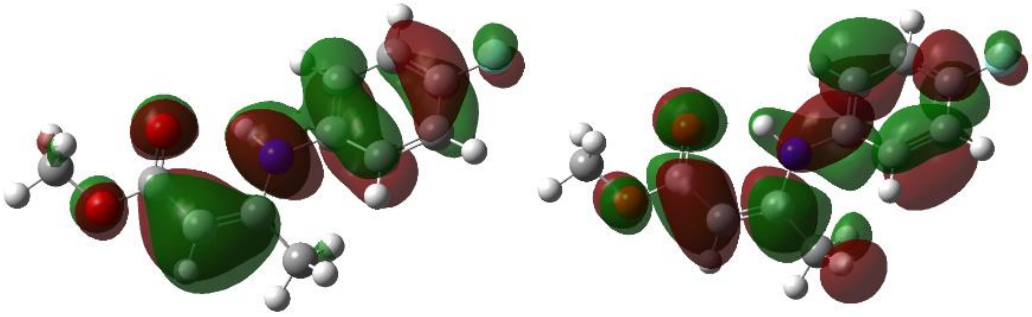

(A) (B)

Figure 5. Electronic densities distribution of HOMO and LUMO of methyl (Z)-3-((4-fluorophenyl) amino) but-2-enoate, calculated at the B3LYP/6-311+G(2d,3p) level of theory.

Frontier molecular orbital energies and molecular electrostatic potential analysis

The main HOMO and LUMO frontiers molecular orbitals were analyzed to study the reactivity of the synthesized compound. Indeed, these frontier orbitals are often linked to the ability of a molecule to give or receive electrons. The HOMO, whose E_{HOMO} energy is high, is a dense orbital, which gives electrons, while the LUMO, characterized by its lowest E_{LUMO} energy, is an orbital poor in electrons, capable of receiving electrons. Figure 5 shows the electronic densities of the HOMO-LUMO orbitals linked to the compound obtained from DFT/B3LYP/6-311+ G(2d,3p) calculations. This Figure indicates that the HOMO is present on the entire molecule, except in the methyl groups. It is especially on the carbon atoms of the phenyl ring and the extra-cyclic double bond that it occurs. Oxygen including their 2pz orbitals, nitrogen and fluorine 2p also play a role in this electron density. These regions are therefore rich electron centers that can interact with the depleted electron centers by electron exchange. Regarding the LUMO, its primary focus is on the heteroatoms' lone pairs and the carbon atoms of the phenyl ring, which are home to the anti-binding p orbitals.

Molecular electrostatic potential analysis

The distribution of the electron density of the studied compound is illustrated by the analysis of the molecular electrostatic potential (MEP)

presented in Figure 6. The nucleophilic centers are represented in red in the regions of high electron density, while the electrophilic centers are represented in blue in the regions of low density. The main nucleophilic centers of our compound are the two oxygen and the fluorine heteroatoms. The electron density is also influenced by the π electrons of the benzene ring as well as the electrons of the extracyclic double bond C=C. The electropositive zones, or electrophilic centers, are mainly located around the hydrogen atoms. The nucleophilic reactivity and the formation of intermolecular hydrogen bonds are favored by these sites.

Table 5 presents the values of the quantum descriptors calculated for the compound studied, which offers valuable information on its chemical reactivity. The ability of a compound to receive an electron is indicated by the electron affinity (A), while the ionization energy (I) makes it possible to determine the chemically reactive atoms in molecules. The FOMs have an energy difference of 4.671 eV. It is difficult to modify hard molecules, which have a high excitation energy, while soft molecules, with low excitation energies, are more reactive and polarizable. The compound is therefore qualified as hard. The chemical potential (μ), which represents the tendency of the electrons to escape from the molecules, is negative for this compound (-3.575 eV), which implies that the compound loses an electron more easily, but gains one more easily. Its electronegativity (χ), slightly higher (χ = 3.575 eV), confirms this. The electrophilic index is an indicator of the decrease in energy due to the maximum transfer of electrons between the donor and the acceptor. The maximum amount of electronic charge that an electrophilic system can accept is given by ΔN_{max}. A good nucleophile has a low electrophilic index value (ω) and a high nucleophilicity value (ε).

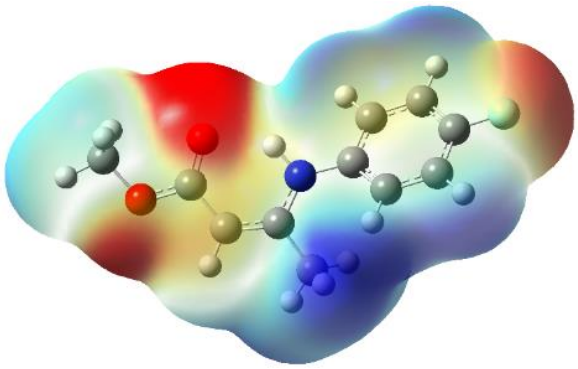

Figure 6. Molecular electrostatic potential of methyl (Z)-3-((4-fluorophenyl) amino) but-2-enoate, calculated at the B3LYP/6-311+G(2d,3p) level of theory.

Table 5. Theoretical parameters for methyl (Z)-3-((4-fluorophenyl) amino) but-2-enoate calculated at B3LYP and 6–311+ G(2d,3p) basis sets

HOMO Energy	E_{HOMO}	-5,910
LUMO Energy	E_{LUMO}	-1,240
HOMO-LUMO Gap energy	ΔEg	4,671
Ionization Potential	I	5,910
Electron Affinity	A	1,240
Electronegativity	χ	3,575
Chemical hardness	η	2,335
Softness	σ	0,428
Chemical potential	μ	-3,575
Electrophilicity index	ω	2,736
Nucleophiliciy	ε	0,365
Additional electronic charge	ΔN_{max}	1,531

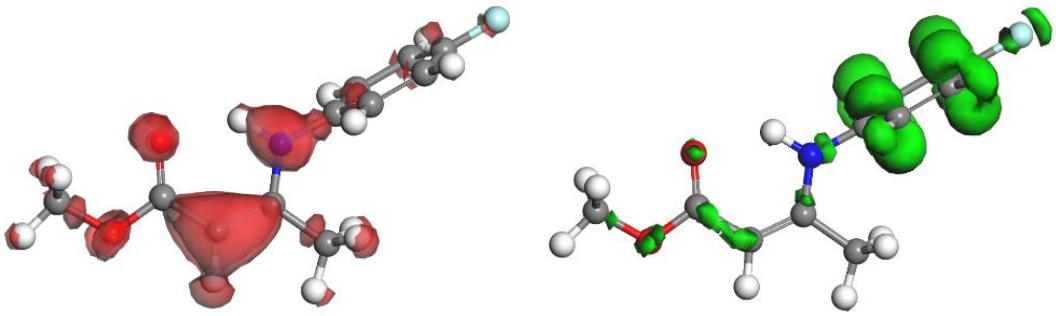

(A) (B)

Figure 7. Fukui functions of the methyl (Z)-3-((4-fluorophenyl) amino) but-2-enoate: a) Fukui f^- and b) Fukui $f+$ functions.

Thus, the compound is more nucleophilic and more electronegative, with a high value of additional charge, allowing it to give more electronic charge (ΔN_{max} = 1.531).

Analysis of local activity indices

An essential and commonly used method for understanding the reactivity and selectivity of an organic molecule is the analysis of local reactivity indices. Using the condensed Fukui functions, derived from the electron density, it becomes easier to predict the sites suitable for an electrophilic or nucleophilic attack. To evaluate the reactivity of the atomic sites and distinguish between electrophilic and nucleophilic attacks, the indices *f*– and *f*+ are calculated. These indices are determined by the following Equation:

$$f^- = q_i(N) - q_i(N-1) \text{ and } f^+ = q(N+1) - q_i(N) \quad (1)$$

Where, q_i is the atomic charge of the i^{th} site in the neutral (N), anionic (N+1), or cationic (N-1) molecule.

For the molecule studied, the condensed indices of the condensed Fukui functions are presented in Table S6 and illustrated in Figure 7. The analysis of these results reveals that the atoms O_2, O_3, N_4, C_{11} and C_{23} are more sensitive to an electrophilic attack, while the atoms C_{19}, C_{21}, C_{24}, and C_{26} are the most susceptible to nucleophilic attacks. These results showed that the distribution of the electrophilic and nucleophilic sites is also in harmony with what was obtained by analyzing the HOMO-LUMO orbitals.

Conclusion

Using spectroscopic methods, a novel enaminoester methyl (Z)-3-((4-fluorophenyl) amino) but-2-enoate has been synthesized and identified. The compound's structure was further characterized by single crystal X-ray Diffraction analysis and ^{1}H-NMR spectrometry. Strong intramolecular hydrogen bonding O···H–N was shown by crystallographic study. The overall Hirshfeld surface is 46.7% contributed by non-classical C-H-H interactions, according to an analysis of near intermolecular interactions. A high-level density functional theory calculation was conducted on the enaminoester compound, revealing a strong correlation with the experimental data. In addition, the frontier molecular orbitals and molecular electrostatic potential were assessed, and both global and local reactivity parameters were calculated and evaluated.

Acknowledgements

We express our heartfelt gratitude to our valued colleagues for dedicating their time and efforts to this report.

Disclosure statement

No potential conflict of interest was reported by the authors in this study.

Orcid

Salima Atlas: 0000-0001-6742-0710
Koffi Senam Etsè: 0000-0001-8495-4327
Abdessamad Tounsi: 0009-0002-0018-6397
Mohamed Anouar Harrad: 0009-0000-0394-1533

References

[1] H.M. Gaber, Z.A. Muhammad, S.M. Gomha, T.A. Farghaly, M.C. Bagley, Recent Synthetic Approaches to N, N-Dimethyl-β-Ketoenamines, *Current Organic Chemistry*, **2017**, *21*, 2168-2195. [Crossref], [Google Scholar], [Publisher]

[2] P.K. Bangalore, S.K. Vagolu, R.K. Bollikanda, D.K. Veeragoni, P.C. Choudante, S. Misra, D. Sriram, B. Sridhar, S. Kantevari, Usnic acid enaminone-coupled 1, 2, 3-triazoles as antibacterial and antitubercular agents, *Journal of Natural Products*, **2019**, *83*, 26-35. [Crossref], [Google Scholar], [Publisher]

[3] N.N. Salama, K.R. Scott, N.D. Eddington, DM27, an enaminone, modifies the in vitro transport of antiviral therapeutic agents, *Biopharmaceutics & Drug Disposition*, **2004**, *25*, 227-236. [Crossref], [Google Scholar], [Publisher]

[4] A.P. Marcus, R. Sarpong, Synthesis of the tetracyclic core of tetrapetalone a enabled by a pyrrole reductive alkyation, *Organic Letters*, **2010**, *12*, 4560-4563. [Crossref], [Google Scholar], [Publisher]

[5] Y.F. Wang, T. Izawa, S. Kobayashi, M. Ohno, Stereocontrolled synthesis of (+)-negamycin from an acyclic homoallylamine by 1, 3-asymmetric induction, *Journal of the American Chemical Society*, **1982**, *104*, 6465-6466. [Crossref], [Google Scholar], [Publisher]

[6] D.L. Boger, T. Ishizaki, R.J. Wysocki Jr, S.A. Munk, P.A. Kitos, O. Suntornwat, Total synthesis and evaluation of (.+-.)-N-(tert-butoxycarbonyl)-CBI,(.+-.)-CBI-CDPI1, and (.+-.)-CBI-CDPI2: CC-1065 functional agents incorporating the equivalent 1, 2, 9, 9a-tetrahydrocyclopropa [1, 2-c] benz [1, 2-e] indol-4-one (CBI) left-hand subunit, *Journal of the American Chemical Society*, **1989**, *111*, 6461-6463. [Crossref], [Google Scholar], [Publisher]

[7] M.A. Harrad, R. Outtouch, M.A. Ali, L. El Firdoussi, A. Karim, A. Roucoux, Ca $(CF_3COO)_2$: An efficient Lewis acid catalyst for chemo- and regio-selective enamination of β-dicarbonyl compounds, *Catalysis Communications*, **2010**, *11*, 442-446. [Crossref], [Google Scholar], [Publisher]

[8] O. Marvi, S. Arshadi, B. Baghernejad, An Efficient Propylphosphonic Anhydride (T3P®)-Mediated MW-induced Solvent-free Rapid Synthesis of Enamino Esters and Ketones including 5, 5-Dimethyl-3-aminocyclohex-2-enones, *Letters in Organic Chemistry*, **2024**, *21*, 541-549. [Crossref], [Google Scholar], [Publisher]

[9] M.A. Harrad, B. Boualy, L. El Firdoussi, M.A. Ali, Aluminum phosphate catalyzed free solvent preparation of β-enamino esters, *American Journal of Chemistry*, **2012**, *2*, 271–276. [Crossref], [Google Scholar], [Publisher]

[10] M.A. Harrad, B. Boualy, I. Houssini, M.A. Ali, Natural phosphate as new highly efficient and reusable heterogeneous catalyst for the selective preparation of *β*-enaminoesters under free-solvent conditions, *Chemistry and Materials Research*, **2014**, *6*, 31–37. [Google Scholar], [Publisher]

[11] Z.H. Zhang, J.Y. Hu, Cobalt (II) chloride-mediated synthesis of beta-enamino

compounds under solvent-free conditions, *Journal of the Brazilian Chemical Society*, **2006**, *17*, 1447-1451. [Crossref], [Google Scholar], [Publisher]

[12] R. Huma, T. Mahmud, N. Idrees, M.J. Saif, R. Munir, N. Akbar, Crystal structure and quantum chemical studies of a novel push–pull enaminone: 3-Chloro-4-((4-bromophenyl) amino) pent-3-en-2-one, *Journal of Chemical Crystallography*, **2020**, *50*, 187-197. [Crossref], [Google Scholar], [Publisher]

[13] K.S. Etsè, G. Zaragoza, K.D. Etsè, Easy preparation of novel 3, 3-dimethyl-3, 4-dihydro-2H-1, 2, 4-benzothiadiazine 1, 1-dioxide: Molecular structure, Hirshfeld surface, NCI analyses and molecular docking on AMPA receptors, *Journal of Molecular Structure*, **2021**, *1238*, 130435. [Crossref], [Google Scholar], [Publisher]

[14] G.M. Sheldrick, Acta Crystallogr, Sect. A: Fundam. Crystallogr, *Structural Chemistry*, **2004**, *64*, 112. [Google Scholar]

[15] G.M. Sheldrick, SHELXT–Integrated space-group and crystal-structure determination, *Acta Crystallographica Section A: Foundations and Advances*, **2015**, *71*, 3-8. [Crossref], [Google Scholar], [Publisher]

[16] A.L. Spek, PLATON SQUEEZE: a tool for the calculation of the disordered solvent contribution to the calculated structure factors, *Acta Crystallographica Section C: Structural Chemistry*, **2015**, *71*, 9-18. [Crossref], [Google Scholar], [Publisher]

[17] L.J. Farrugia, WinGX and ORTEP for Windows: an update, *Journal of Applied Crystallography*, **2012**, *45*, 849-854. [Crossref], [Google Scholar], [Publisher]

[18] L.J. Farrugia, WinGX and ORTEP for Windows: an update, *Journal of Applied Crystallography*, **2012**, *45*, 849-854. [Crossref], [Google Scholar], [Publisher]

[19] C.F. Macrae, I.J. Bruno, J.A. Chisholm, P.R. Edgington, P. McCabe, E. Pidcock, L. Rodriguez-Monge, R. Taylor, J. Streek, P.A. Wood, Mercury CSD 2.0–new features for the visualization and investigation of crystal structures, *Journal of Applied Crystallography*, **2008**, *41*, 466-470. [Crossref], [Google Scholar], [Publisher]

[20] R.H. Hertwig, W. Koch, On the parameterization of the local correlation functional. What is Becke-3-LYP?, *Chemical Physics Letters*, **1997**, *268*, 345-351. [Crossref], [Google Scholar], [Publisher]

[21] M.J. Frisch, D.J. Fox, Gaussian 09, C3 Revision B.01, Gaussian Inc, **2010**. Walling-form CT.

[22] M. Adardour, M. Lasri, M. Ait Lahcen, M. Maatallah, R. Idouhli, M.M. Alanazi, S. Lahmidi, A. Abouelfida, J.T. Mague, A. Baouid, Exploring the efficacy of benzimidazolone derivative as corrosion inhibitors for copper in a 3.5 Wt.% NaCl solution: a comprehensive experimental and theoretical investigation, *Molecules*, **2023**, *28*, 6948. [Crossref], [Google Scholar], [Publisher]

[23] K. El Gadali, M. Rafya, M. Maatallah, A. Mehdi, A. Ouahrouch, F. Benkhalti, Y.S. Sanghvi, M. Taourirte, H.B. Lazrek, Synthesis, structural characterization and antibacterial activity evaluation of novel quinolone-1, 2, 3-triazole-benzimidazole hybrids, *Journal of Molecular Structure*, **2023**, *1282*, 135179. [Crossref], [Google Scholar], [Publisher]

[24] M. Lasri, M. Fawzi, O. Zakir, A. Hasnaoui, R. Idouhli, M. Maatallah, K. Mohyeddine, M.Y.A. Itto, A. Auhmani, A. Abouelfida, Exploring the effectiveness of two triazole derivatives as copper corrosion inhibitors in NaCl solution: a combined approach of quantitative chemistry and dynamic molecular simulations, *Journal of Molecular Structure*, **2024**, *1303*, 137593. [Crossref], [Google Scholar], [Publisher]

[25] K. Wolinski, J.F. Hinton, P. Pulay, Efficient implementation of the gauge-independent atomic orbital method for NMR chemical shift calculations, *Journal of the American Chemical*

Society, **1990**, *112*, 8251-8260. [Crossref], [Google Scholar], [Publisher]

[26] M.J. Turner, J.J. McKinnon, S.K. Wolff, D.J. Grimwood, P.R. Spackman, D. Jayatilaka, M.A. Spackman, CrystalExplorer17, The University of Western Australia, **2017.** [Publisher]

[27] P.R. Spackman, M.J. Turner, J.J. McKinnon, S.K. Wolff, D.J. Grimwood, D. Jayatilaka, M.A. Spackman, CrystalExplorer: a program for Hirshfeld surface analysis, visualization and quantitative analysis of molecular crystals, *Journal of Applied Crystallography*, **2021**, *54*, 1006-1011. [Crossref], [Google Scholar], [Publisher]

[28] F. Hirshfeld, Electron density distributions in molecules, *Crystallography reviews*, **1991**, *2*, 169-200. [Crossref], [Google Scholar], [Publisher]

[29] M.A. Spackman, J.J. McKinnon, Fingerprinting intermolecular interactions in molecular crystals, *CrystEngComm*, **2002**, *4*, 378-392. [Crossref], [Google Scholar], [Publisher]

HOW TO CITE THIS ARTICLE

S. Atlas, K.S. Etsè, Z.V. Guillermo, M. Maatallah, A. Tounsi, M.A. Harrad. Structural and Quantum Study of Newly Synthesized Methyl(Z)-3-((4-Fluorophenyl) Amino) But-2-Enoate. *Adv. J. Chem. A*, 2025, 8(4), 809-824.

DOI: 10.48309/AJCA.2025.471262.1623
URL: https://www.ajchem-a.com/article_207875.html